Acta Oceanol. Sin., 2025, Vol. 44, No. 3, P. 147–160
https://doi.org/10.1007/s13131-025-2474-4

Influence of grounding giant iceberg D15 on sea ice and polynyas in a sea ice-ice shelf-ocean numerical model of the Prydz Bay, Antarctica

Quanyi Zhou[1, 2], Jiuxin Shi[1, 2*], Chuning Wang[3], Longjiang Mu[4], Zhigang Yao[1, 2], Zhaoru Zhang[3], Yuxin Han[1, 2], Yongming Sun[1, 2]

[1] Physical Oceanography Laboratory, Ocean University of China, Qingdao 266100, China

[2] Laboratory for Ocean Dynamics and Climate, Qingdao Marine Science and Technology Center, Qingdao 266237, China

[3] Key Laboratory of Polar Ecosystem and Climate Change, Ministry of Education and School of Oceanography, Shanghai Jiao Tong University, Shanghai 200030, China

[4] Laoshan Laboratory, Qingdao 266237, China

Received 16 October 2024; accepted 24 March 2025

© Chinese Society for Oceanography and Springer-Verlag GmbH Germany, part of Springer Nature 2025

Abstract

A three-dimensional coupled sea ice-ice shelf-ocean numerical model is developed for the Prydz Bay, Antarctica, using the Regional Ocean Modeling System with a grid resolution of approximately 2 km. The influence of the grounding giant iceberg D15 on the distribution of sea ice and polynyas in the Prydz Bay is analyzed through two numerical experiments. Iceberg D15, grounded off the western edge of the West Ice Shelf (WIS), obstructs the southwestward transport of sea ice along the east coast of Prydz Bay, causing sea ice to accumulate to the east of the iceberg and form multi-year fast ice. Grounding of Iceberg D15 also decreases sea ice coverage off its south edge and creates ice-free openings in spring near Davis Station and Zhongshan Station, facilitating the accessibility of vessels to the research stations. These simulated sea ice patterns closely match current satellite observations. When Iceberg D15 is removed, the previously blocked sea ice north of the iceberg, which moved westward, shifts southwesterly along the coastline, leading to a reduction in sea ice thickness during winter and spring, as well as lower sea ice concentrations in spring across large areas north and west of the iceberg. In contrast, the sea ice thickness increases considerably southwest of the WIS, extending to the front of the Amery Ice Shelf during seasons covered by sea ice. The increase in sea ice concentration can also extend to as far as 75°E in spring. Without Iceberg D15, which previously contributed to the ice barrier of Barrier Polynya (BP), the shape of BP changes, the area of BP and Davis Polynya (DP) decreases, and the polynya off the northwest edge of the WIS near 83°E expands. These polynya patterns are much similar to the satellite remote sensing observations before Iceberg D15 was grounded. From April to October, the total area of BP and DP decreases by 2.83×10^4 km^2 (60%) and 2.20×10^3 km^2 (20%), respectively, while the total sea ice production decreases by 4.11×10^{10} m^3 (66%) and 1.52×10^{10} m^3 (52%) compared to the experiment with iceberg. These results indicate the substantial effects of grounding giant icebergs on the spatio-temporal distribution of sea ice, the area of polynyas, and sea ice production. High-resolution Antarctic coastal numerical models, typically with grid scales of kilometers, are sufficient to represent large icebergs, and adding the grounding giant icebergs is crucial for producing realistic simulations of sea ice and polynyas.

Key words grounding iceberg, sea ice, polynya, numerical simulation, Prydz Bay, Antarctica

Citation Zhou Quanyi, Shi Jiuxin, Wang Chuning, Mu Longjiang, Yao Zhigang, Zhang Zhaoru, Han Yuxin, Sun Yongming. 2025. Influence of grounding giant iceberg D15 on sea ice and polynyas in a sea ice-ice shelf-ocean numerical model of the Prydz Bay, Antarctica. Acta Oceanologica Sinica, 44(3): 147–160, doi: 10.1007/s13131-025-2474-4

Foundation item: The National Natural Science Foundation of China under contract Nos 41976217 and 42306249; the National Key Research and Development Program of China under contract No. 2018YFA0605701.

*Corresponding author, E-mail: shijiuxin@ouc.edu.cn

1 Introduction

The Prydz Bay, the third largest bay in Antarctica, has been a central region for Chinese polar marine scientific research (Shi et al., 2013; Gao et al., 2016). The coastline of the bay is shaped by the two ice shelves along its shores: the Amery Ice Shelf (AIS), the largest ice shelf in East Antarctica, situated in the southwest corner of the bay, and the West Ice Shelf (WIS), located to the northeast, outside the bay (Fig. 1). The bay exhibits varied topography, with the Four Ladies Bank (FLB) on the east side of the entrance of the bay, and the Fram Bank to the west, where the depth is less than 200 m at its shallowest. Between these two banks lies the Prydz Channel, which is the main channel for water exchange between the bay and the open ocean.

The circulation system in the Prydz Bay consists of the east-to-west Antarctic Slope Current (ASC) along the continental slope and the cyclonic Prydz Bay Gyre (PBG) within the bay (Fig. 1). These patterns have been observed through summer dynamical height analyses (Smith et al., 1984; Nunes Vaz and Lennon, 1996) and validated through numerical models (Shi et al., 2000, 2002; Aoki et al., 2010; Galton-Fenzi et al., 2012). Liu et al. (2017) identified a strong southwesterly coastal current, the Prydz Bay Eastern Coastal Current (PBECC), flowing along the coast between 75°E and 82°E, further confirmed by recent numerical simulations for summer (Han et al., 2022).

The seasonal cycle of sea ice in the Prydz Bay is distinct, with the minimum extent occurring in late February when ice is mainly concentrated near the east and west coasts and the shallows at the entrance of the bay. In September, the sea ice reaches its peak coverage, extending northward beyond 60°S (Zheng and Shi, 2011). Analysis of satellite-derived sea ice concentration data from 1987 to 1994 identified several winter polynyas across the Prydz Bay from west to east, including the Mackenzie Polynya (MP), the AIS Polynya (AISP), the Prydz Polynya [later referred to as the Davis Polynya (DP) by Williams et al. (2016)], the Barrier Polynya (BP), and the West Ice Shelf Polynya (WISP) (Massom et al., 1998). However, subsequent studies revealed that AISP had vanished, while new offshore polynyas formed near the FLB (Tamura et al., 2008, 2016; Nihashi and Ohshima, 2015; Lin et al., 2024). Recent research has further classified these polynyas, including the Iceberg D15 Polynya (ID15P) and FLB Polynya (FLBP). The DP located beyond the extent of landfast ice, is similarly categorized as an offshore polynya (Hou and Shi, 2021).

Drifting icebergs, often driven by ocean currents into the interior of the Prydz Bay, frequently ground in the shallow areas of the FLB (water depths below 200 m) (Li et al., 2017). Grounding giant icebergs can profoundly im-

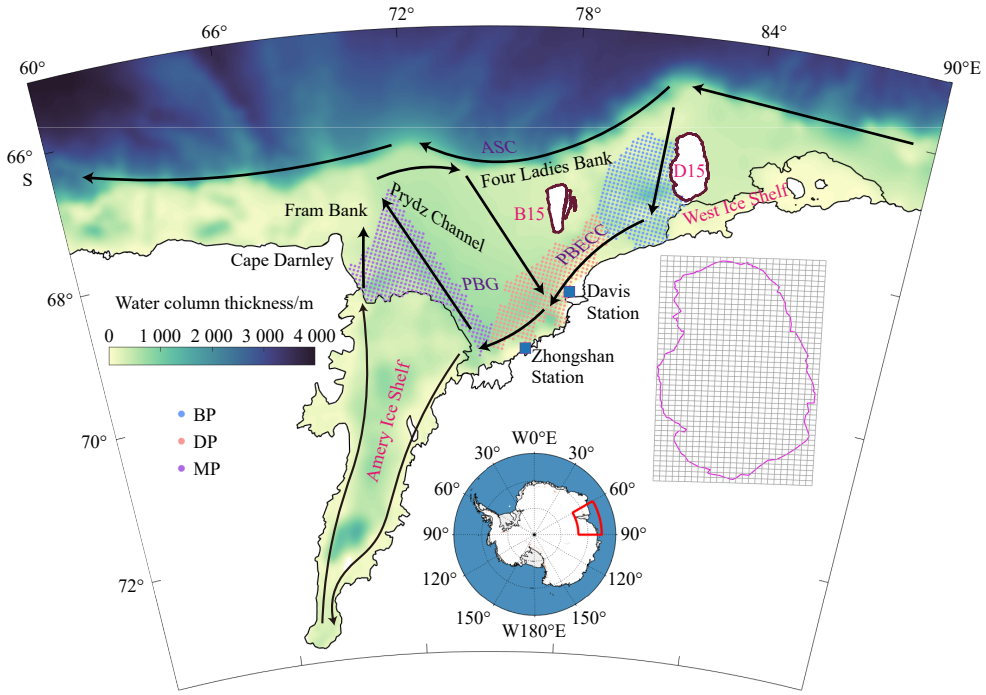


Fig. 1. Water column thickness of the Prydz Bay and surrounding areas in the model. Red lines represent the outline of Icebergs D15 and B15. Colored dots represent the mask of the Barrier Polynya (BP), Davis Polynya (DP), and Mackenzie Polynya (MP) in Prydz Bay from April to October from 2003 to 2020 (Hou, 2022), derived from remote sensing thin ice thickness data retrieved from satellite remote sensing. Black arrows represent major circulation in the bay. Blue squares indicate the research stations. Gray grid represents the model grid at Iceberg D15, shown in the inset on the right. The lower inset shows Antarctica and the surrounding Southern Ocean, with the red box indicating the Prydz Bay. ASC: Antarctic Slope Current; PBG: Prydz Bay Gyre; PBECC: Prydz Bay Eastern Coastal Current.

pact the sea ice distribution by obstructing its movement (Dinniman et al., 2007). Hou and Shi (2021) reported that a group of grounding giant icebergs, B15 (consisting of Icebergs B15t, B15b, and B15r), substantially increased the size of the ice barrier on the eastern side of the FLBP, which effectively blocked sea ice transport from the BP to the open ocean. This obstruction led to the closure of the BP in mid-September of 2008. The lack of sea ice outflow from the BP resulted in the merging of the FLBP and DP, creating a much larger polynya and increasing the areas of the original polynyas. Additionally, Iceberg D15, grounded between the southeast side of the FLB and the northwest side of the WIS since 1991 (Wesche and Dierking, 2015; Hou and Shi, 2021), has a remarkable influence on the summer circulation in the Prydz Bay. A numerical model showed that its presence obstructs the current off the northern edge of the WIS and enhances the ASC branch entering the bay along the western edge of the WIS (Han et al., 2022).

Previous sea ice numerical simulations (Li et al., 2011; Liu et al., 2017) typically indicated minimal to no sea ice presence in the Prydz Bay during summer. While the MP is accurately simulated in winter, the DP and BP are often simulated as a single polynya, likely due to the absence of Iceberg D15 in these model configurations. Therefore, this study aims to address this problem by investigating the impact of Iceberg D15 on sea ice and polynyas simulations through conducting numerical experiments that include and exclude this iceberg from the model topography.

2 Model description and validation

2.1 *Model description*

Regional Ocean Modeling System (ROMS) is a widely employed three-dimensional, terrain-following primitive equation ocean model with a free surface (Shchepetkin and McWilliams, 2005). In this study, we adopt a modified version of ROMS including sea-ice and ice-shelf models developed by Wang et al. (2024). The sea ice model is mainly based on Budgell (2005), which combines the elastic-viscous-plastic (EVP) rheology (Hunke and Dukowicz, 1997; Hunke, 2001) with a simple one-layer ice and snow thermodynamic model, including a molecular sublayer under the ice (Mellor and Kantha, 1989). The ice shelf model follows Galton-Fenzi et al. (2012) and employs a three-equation thermodynamic scheme.

The model domain covers the entire Prydz Bay, including the AIS and WIS (65°–73.5°S, 60°–90°E), with a zonal resolution of 1/18°. The grid spacing varies from 1.75 km (southern boundary) to 2.6 km (northern boundary), with an average of 2.16 km. A 32-layer terrain-following σ-coordinate system is adopted in the vertical direction, with higher vertical resolution near the surface (4.9 m to 10.5 m). Bathymetry and ice-shelf draft data are derived from the global 30′ high-resolution RTopo-2 dataset, as used by Han et al. (2022), and are smoothed using a Shapiro filter.

The eastern, western, and northern boundaries are open and positioned far from the Prydz Bay to diminish boundary effects. Boundary conditions for salinity, potential temperature, ocean velocities, sea surface height, sea ice concentration, sea ice thickness, snow thickness, and sea ice velocities are from monthly averaged data (2013–2018) from Oceanic General Circulation Model (OGCM) for the Earth Simulator (OFES) version 2. These datasets are averaged over six years to obtain monthly values. A sponge layer is applied at the western and northern open boundaries to maintain model stability.

Atmospheric forcing, including 10-m wind speed, 2-m surface air pressure, 2-m relative humidity, downward shortwave radiation, longwave radiation, and total precipitation rates derived from the fifth generation European Centre for Medium-Range Weather Forecast (ECMWF) (ERA-5) reanalysis product from 2013 to 2018, processed into daily averages over six years. The bulk flux parameterization scheme of Large and Yeager (2009) calculates wind stress, heat fluxes, and freshwater fluxes. The downward shortwave radiation is adjusted for albedo correction, and sea ice albedo is calculated using the community sea ice model (CSIM) algorithm. The initial conditions are set using the January average potential temperature and salinity for 2013–2018 from OFES version 2, while ocean velocities, sea ice concentration, and sea ice velocities are set to zero. The model time step is 120 s, reaching a steady state after three years of integration. Our analysis is based on monthly means from the eighth year of the simulation.

Two experiments are designed for comparison (Table 1). Experiment 1 (Exp. 1) represents present-day conditions including Iceberg D15, while Experiment 2 (Exp. 2) excludes it. Iceberg D15 has been grounded on the western side of the WIS since 1991, exhibiting no detectable changes in shape or position, indicating negligible melting (Hou and Shi, 2021). Given its minimal thermodynamic impact on circulation and sea ice, the iceberg is treated as land in the model, with a constant outline extracted from a visible image captured by the Moderate Resolution Imaging Spectroradiometer (MODIS) onboard the Terra satellite (Han et al., 2022).

2.2 *Model validation*

The reliability of the model is validated using results from Exp. 1. The simulated circulation for February is compared with the Acoustic Doppler Current Profiler (ADCP) observations from the 31st Chinese Antarctic

Table 1. Configuration of the numerical experiments

Experiment	Configuration
Exp. 1	with Iceberg D15
Exp. 2	without Iceberg D15

Expedition (12 February to 3 March 2015). The 38 kHz ADCP used during the expedition can provide data for depths shallower than 800 m, although the comparisons are restricted to depths above 420 m due to the declining reliability with depth. Simulated summer circulation patterns are generally consistent with the ADCP observations (Fig. 2), reproducing the presence of cyclonic gyres PBG, and align well with the simulations of Han et al.

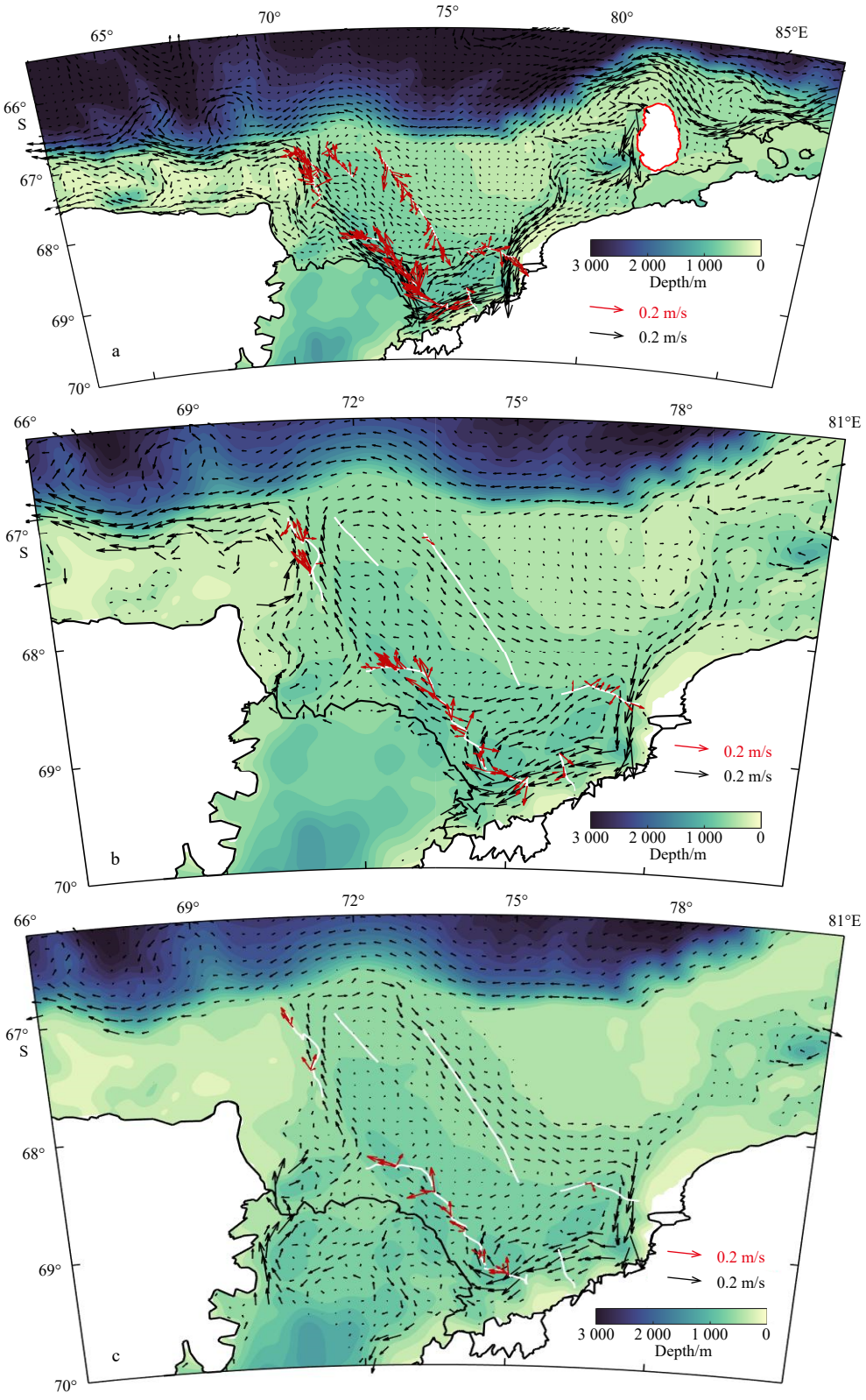


Fig. 2. Comparison of circulation in Exp. 1 with ADCP observations at depths of 50 m (a), 210 m (b), and 420 m (c) in February. Red arrows represent ADCP observations, while black arrows represent Exp. 1 results. ADCP: Acoustic Doppler Current Profiler.

(2022). Additionally, a smaller cyclonic gyre is identified east of the ice shelf front near 69°S in southeastern Prydz Bay, flowing northeastward and merging into the PBECC. This feature appears throughout the water column, with ADCP measurements at 210 m and 420 m supporting its presence.

Sea ice model validation is conducted using multi-year average sea ice concentration data from the Advanced Microwave Scanning Radiometer 2 (AMSR-2) for the 2013–2018 period. Comparisons of the monthly average sea ice area show consistency with AMSR-2 data (Fig. 3), capturing seasonal cycles marked by a February minimum, a subsequent increase in March, and complete ice cover from April through September. This variation is also consistent with remote sensing observations (Zheng and Shi, 2011). The spatial distribution of sea ice concentration (Fig. 4) in the representative months of the four seasons (February, May, August, and November) is also generally consistent with the AMSR-2 pattern (Fig. 5). In February, the Prydz Bay exhibits minimal sea ice, limited

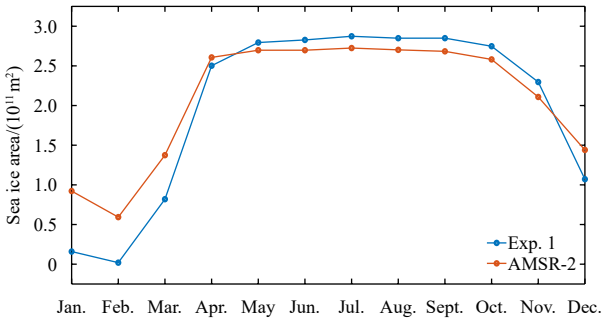


Fig. 3. Comparison of sea ice areas in Exp. 1 and AMSR-2. AMSR-2: Advanced Microwave Scanning Radiometer 2.

to the southeastern region near Iceberg D15 and the WIS junction (Fig. 4a). As temperatures drop in autumn, ice formation begins in March, resulting in widespread coverage by May (Fig. 4b). By August, nearly the entire bay is ice-covered, with a few coastal polynyas remaining (Fig. 4c). Melting starts in November, leading to significantly reduced concentrations in the coastal areas while the rest of the bay remains ice-covered (Fig. 4d).

In summer, the simulated sea ice area is lower than the AMSR-2 data (Fig. 5a), with lower concentrations to the east and north of Iceberg D15, in northern FLB, east of the AIS, and east of Cape Darnley. These regions typically have fast ice formed by small grounding icebergs acting as anchors (Hou and Shi, 2021). The discrepancy between Exp. 1 and the remote sensing data is primarily due to the absence of fast ice formation algorithms, particularly those involving small grounding icebergs critical to fast ice formation offshore, which is a common limitation in current Antarctic sea ice models (Van Achter et al., 2022).

Four coastal polynyas are identified in Exp. 1 which are BP, MP, DP, and Cape Darnley Polynya (CDP) (Fig. 4c). These simulated polynyas are generally in good agreement with the locations and sizes observed in remote sensing data (Hou and Shi, 2021). The current model has a significant improvement over previous efforts (Li et al., 2011; Liu et al., 2017) by clearly distinguishing BP from DP, which are collectively referred to as the Prydz Polynya in earlier models. Despite this advancement, some discrepancies remain. While remote sensing data show DP is situated offshore (north of the fast ice near the Davis Station), Exp. 1 depicts DP tightly bound to the coast. Additionally, Exp. 1 fails to reproduce the offshore

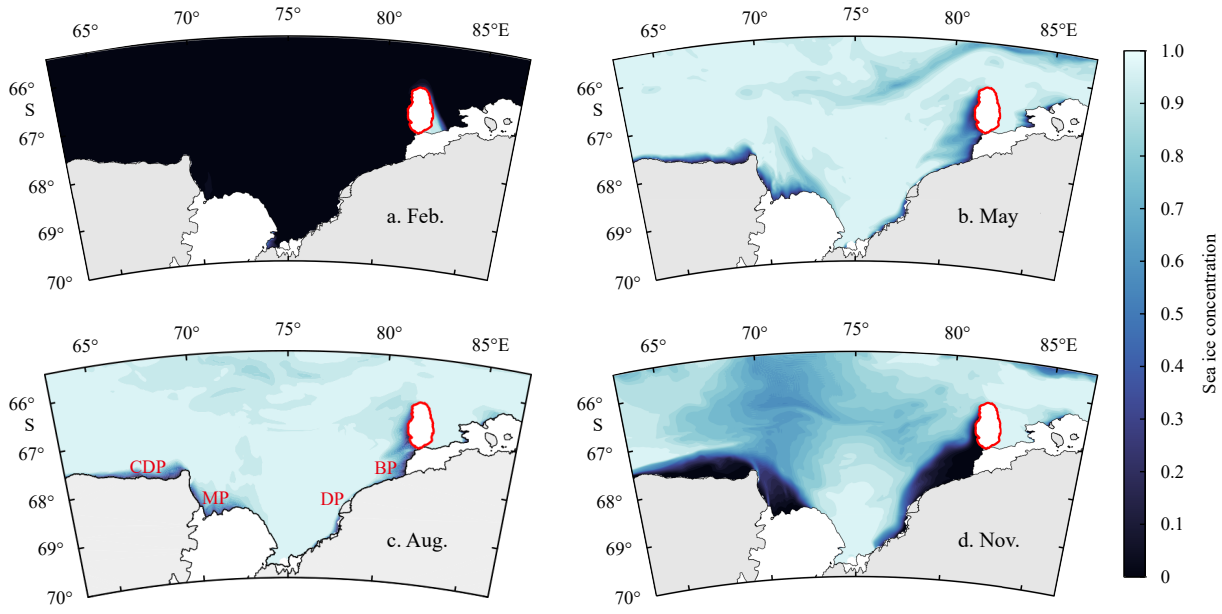


Fig. 4. Sea ice concentration during typical months of the four seasons in Exp. 1. a. February, b. May, c. August, and d. November. The closed red curve represents Iceberg D15, and polynyas that emerge in winter in the model are labeled in red font. CDP: Cape Darnley Polynya; MP: Mackenzie Polynya; DP: Davis Polynya; BP: Barrier Polynya.

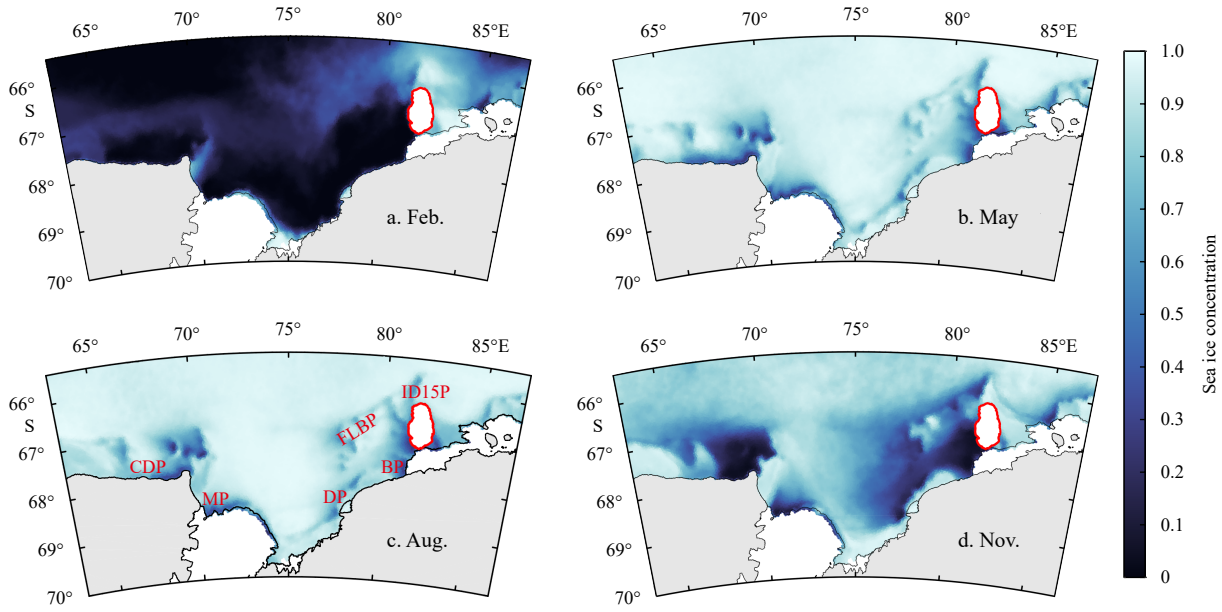


Fig. 5. Sea ice concentration during representative months of the four seasons in AMSR-2. a. February, b. May, c. August, d. November. The closed red curve represents Iceberg D15, and polynyas that emerge in winter in the model are labeled in red font. CDP: Cape Darnley Polynya; MP: Mackenzie Polynya; DP: Davis Polynya; BP: Barrier Polynya.

ID15P and the FLBP (Fig. 5c), which are both formed by the breaking of fast ice anchored to small grounding icebergs (Hou and Shi, 2021). These differences are likely due to the limitation of the current model in simulating fast ice. Furthermore, remote sensing reveals detailed spatial variability in polynya structure compared to smoother patterns in the model outputs, which may also account for these differences.

Direct comparisons of sea ice thickness and velocities are not feasible due to the lack of comprehensive data. However, the simulated sea ice thickness (Fig. 6) captures seasonal variations in the Prydz Bay, with lower ice thickness areas co-located at the identified coastal polynyas, particularly during winter. Thick multi-year ice (exceeding 2 m) persists year-round off the eastern edge of Iceberg D15, remaining present even during summer. Sea ice velocity patterns (Fig. 7) indicate enhanced movements along the ASC, the PBECC, and the coastal areas associated with the PBG, consistent with observed circulation features.

To validate the model performance in polynya areas, simulated monthly mean polynya areas from April to October are compared with those derived from remote sensing thin ice thickness (TIT) data (Hou, 2022), based on the methods described by Nihashi and Ohshima (2015) and Nihashi et al. (2017). Polynya areas are determined using daily mean ice thickness data, with regions where ice is thinner than 0.2 m classified as polynyas within the defined polynya mask (Fig. 1). Due to the absence of fast ice representation in the model, the simulated sea ice concentrations during autumn are lower than those observed in remote sensing data, leading to larger areas of thin ice in April and, consequently, larger areas for polynyas. While the simulated areas of BP and their monthly trend generally agree with the observations, DP areas are underestimated due to the missing ice barrier formed by fast ice. In contrast, MP appears larger than observed, likely because the model does not account for fast ice near Cape Darnley (Table 2, Fig. 8a).

Sea ice production (SIP) estimates from the model are compared with remote sensing estimates for BP, DP, and MP within the defined polynya mask (Fig. 1) (Hou, 2022). It is important to note the methodological differences between the calculation of SIP: the model accounts for potential melting driven by ocean thermodynamics (Mellor and Kantha, 1989), whereas the satellite-derived algorithm, based on TIT data, employs a heat budget approach which assumes no oceanic heat flux and all heat loss in the polynya is caused by ice formation. It further balances radiative and turbulent fluxes at the ice surface with conductive heat flux in the ice. The ice surface temperature is determined using empirical formulas for radiative and turbulent fluxes, which then allows the heat loss to be calculated as the conductive heat flux (Ohshima et al., 2016; Lin et al., 2023). For consistency, SIP comparisons are restricted to April through October, when sea ice melt is minimal. Overall, the total SIP (Table 2) and its temporal trend (Fig. 8b) for BP and DP are in good agreement with remote sensing estimates, except for MP, where the absence of fast ice introduces bias. Notably, the model accurately captures decreasing SIP of BP from June to July while depicting the stable SIP conditions for DP from June to August.

In conclusion, the Exp. 1 simulation effectively repro-

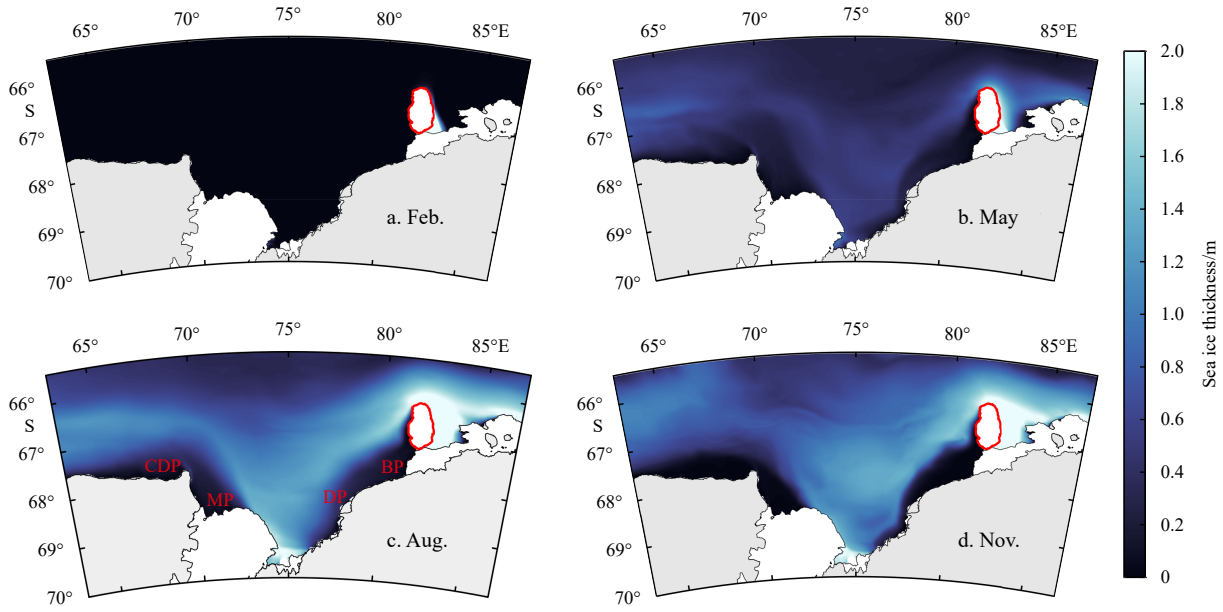


Fig. 6. Sea ice thickness for representative months of the four seasons in Exp. 1. a. February, b. May, c. August, and d. November. The closed red curve represents Iceberg D15, and polynyas that emerge in winter in the model are labeled in red font. CDP: Cape Darnley Polynya; MP: Mackenzie Polynya; DP: Davis Polynya; BP: Barrier Polynya.

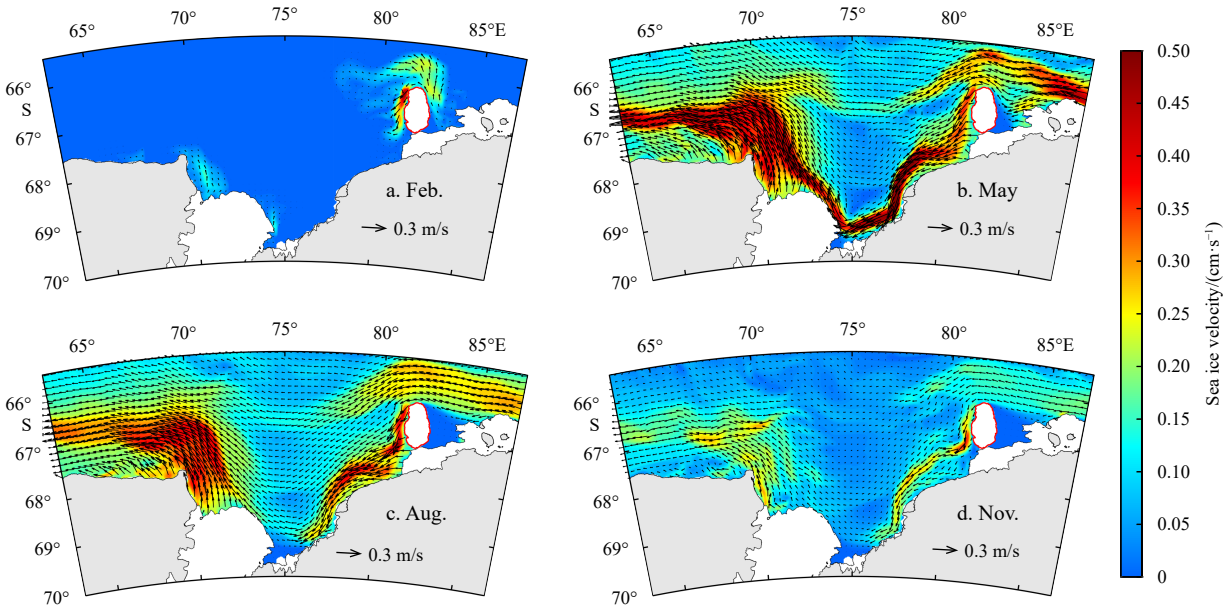


Fig. 7. Sea ice velocities for representative months of the four seasons in Exp. 1. a. February, b. May, c. August, and d. November. The closed red curve represents Iceberg D15.

Table 2. Total area and sea ice production (SIP) of the Barrier Polynya (BP), Davis Polynya (DP), and Mackenzie Polynya (MP) in Prydz Bay in April–October, in remote sensing (RS), Exp. 1, and Exp. 2 results

Method	Total area/(10^4 km^2)			Total SIP/(10^{10} m^3)		
	BP	DP	MP	BP	DP	MP
RS	4.80	2.64	3.20	6.32	2.92	6.59
Exp. 1	4.70	1.09	4.62	6.28	2.91	10.98
Exp. 2	1.87	0.87	4.49	2.17	1.39	10.61

duces the realistic circulation patterns, annual sea ice area variability, sea ice concentration distributions, major polynya locations, and SIP variability in the Prydz Bay. The sea ice-ice shelf-ocean model developed in this study thus demonstrates robust performance in simulating circulation, sea ice dynamics, and polynyas in the region.

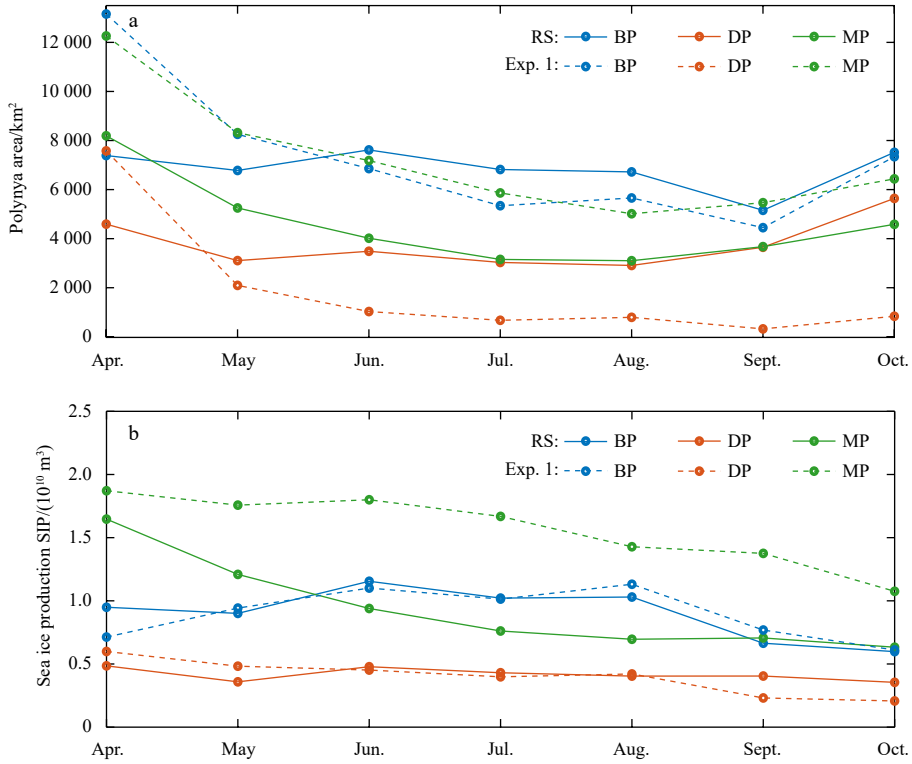


Fig. 8. Areas (a) and sea ice production (SIP) (b) of BP, DP, and MP for April–October in Remote Sensing (RS) and Exp. 1 results, calculated within the polynya mask shown in Fig. 1. SIP: sea ice production; BP: Barrier Polynya; DP: Davis Polynya; MP: Mackenzie Polynya.

3 Results and discussion

In the Exp. 2 simulation, removing Iceberg D15 leads to near-complete absence of sea ice in the Prydz Bay region during summer (Fig. 9a and 10a), consistent with previous numerical modeling studies (Li et al., 2017). During the other three seasons, sea ice covers the region formerly occupied by Iceberg D15. A larger region of low sea ice thickness and concentration emerges between the northwestern edge of the WIS and the grounding position of D15, approximately at 83°E. This indicates an expansion of the polynya in this area, with its extent persisting

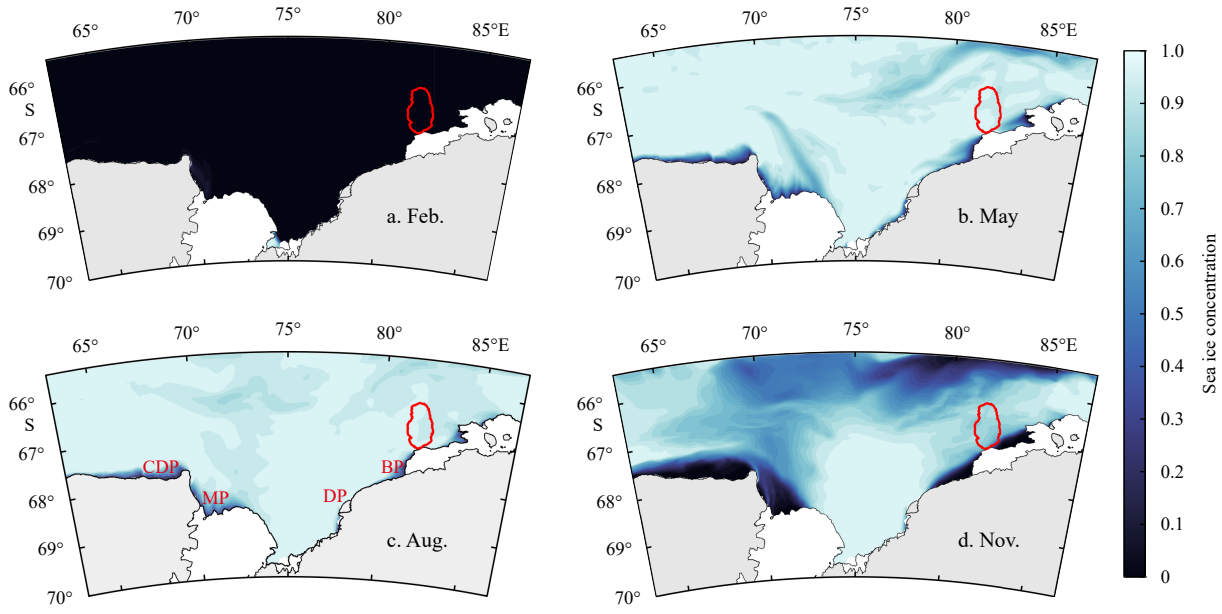


Fig. 9. Sea ice concentration in representative months of the four seasons in Exp. 2. a. February, b. May, c. August, and d. November. The closed red curve represents Iceberg D15, and polynyas that emerge in winter in the model are labeled in red font. CDP: Cape Darnley Polynya; MP: Mackenzie Polynya; DP: Davis Polynya; BP: Barrier Polynya.

through both autumn and winter, as the WIS serves as an ice barrier (Figs 9c and 10c). Another area of low sea ice concentration and thickness forms around 80°E, coinciding with deformed BP, whose barrier shifts to the western WIS following the loss of its former barrier provided by Iceberg D15 (Figs 9c and 10c). This pattern of polynya distribution closely matches previous numerical modeling results and is close to pre-1990 remote sensing observations (Massom et al., 1998).

During winter and spring, sea ice with thickness exceeding 1 m emerges in the polynya areas southwest of the previous D15, extending to the eastern edge of AIS, while sea ice over 2 m thick is found near 75°E off the east edge of AIS. However, areas of low sea ice thickness appear in the north part of the bay, i.e., at FLB and the Prydz Channel (Figs 10c and d). In spring, extensive areas of low sea ice concentration span across 70°–85°E in the northern part of the Prydz Bay (Fig. 9d).

Removing Iceberg D15 eliminates the multi-year fast ice that previously accumulated to its east during summer (Fig. 11a). In autumn, sea ice concentration changes are limited, with a slight decrease off the eastern edge of D15 where it meets the WIS, and a small increase to the west (Fig. 11b). Without D15, ice thickness slightly reduces to the east, spreading north and west of the iceberg (Fig. 12b), while slight increase is noted to the southwest.

In winter, the sea ice concentration falls slightly to the east of Iceberg D15 at the front of the WIS, while increasing to the west, where the iceberg no longer obstructs sea ice movement (Fig. 11c). More remarkable changes in thickness emerge, with substantial increases extending southwest along the Prydz Bay coastline, reaching the northern front of the AIS (72°E) and further northwest to approximately 70°E. In contrast, a decrease in ice thickness is observed east and north of the iceberg, spreading westward to the FLB and the Prydz Channel, reaching around 70°E (Fig. 12c). Overall, the removal of Iceberg D15 eliminates its role as an ice barrier, leading to the loss of the sea ice accumulation zone to the east and widespread reduction in thickness in the FLB and the northern part of the bay. Open water areas decrease southwest of the iceberg and the WIS, while the ice barrier of the BP shifts to the western WIS, changing the shape of the BP and reducing the area of the BP and DP.

In spring, increased sea ice concentration extends southwest from the former iceberg position along the coastline to around 75°E (Fig. 11d), whereas declines occur east of the iceberg. A substantial reduction is also evident to the north, extending from 85°E to 70°E (Fig. 11d). The spring decrease in sea ice thickness along the continental slope west of the iceberg is more substantial compared to winter (Fig. 12d). Simulated ice velocities suggest that the reduction in sea ice concentration to the north of Iceberg D15 in spring, as well as the large-scale increases in sea ice thickness to the north and west in winter and spring, results from changed transport pathways following the removal of the iceberg. Sea ice that once moved along the north edge of the iceberg now moves southwestward along the WIS front (Fig. 13).

The polynya distributions in Exp. 1 and Exp. 2 differ primarily around the WIS. In Exp. 2 (Fig. 10), the northern boundary of the BP retreats remarkably, shifting into the southeast corner where the WIS meets the coastline. Another polynya, situated along the northwest edge of the WIS near 83°E, has expanded in this region. This pattern is consistent with the observations by Massom et al. (1998) based on satellite remote sensing sea ice concentration data from 1987 to 1994, suggesting these observa-

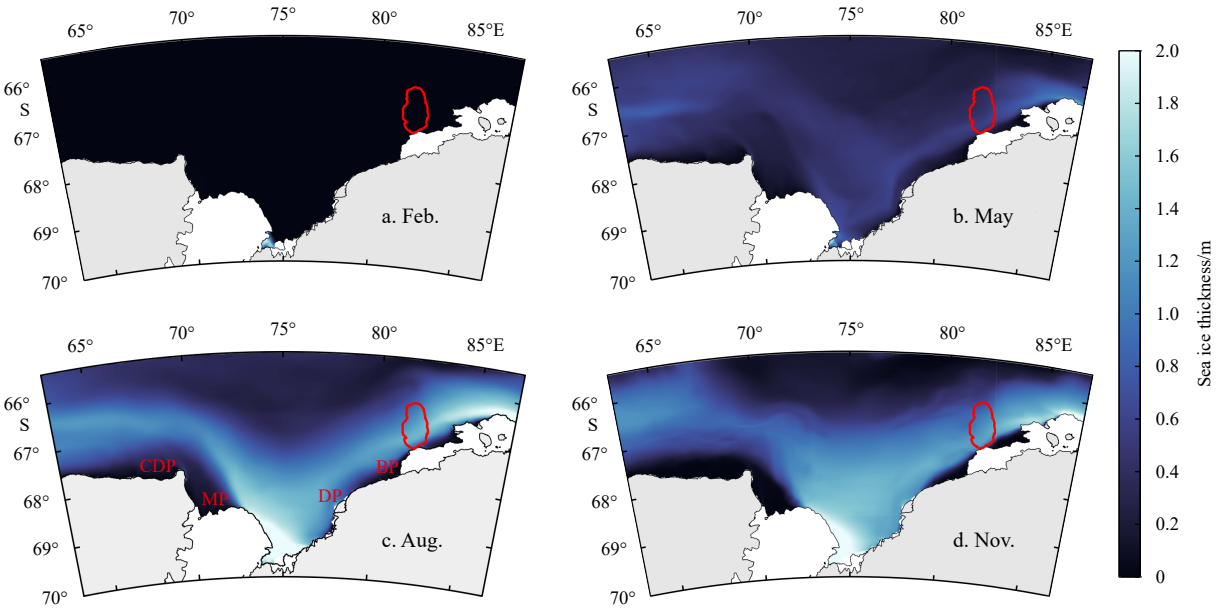


Fig. 10. Sea ice thickness in representative months of the four seasons in Exp. 2. a. February, b. May, c. August, and d. November. The closed red curve represents Iceberg D15, and polynyas that emerge in winter in the model are labeled in red font. CDP: Cape Darnley Polynya; MP: Mackenzie Polynya; DP: Davis Polynya; BP: Barrier Polynya.

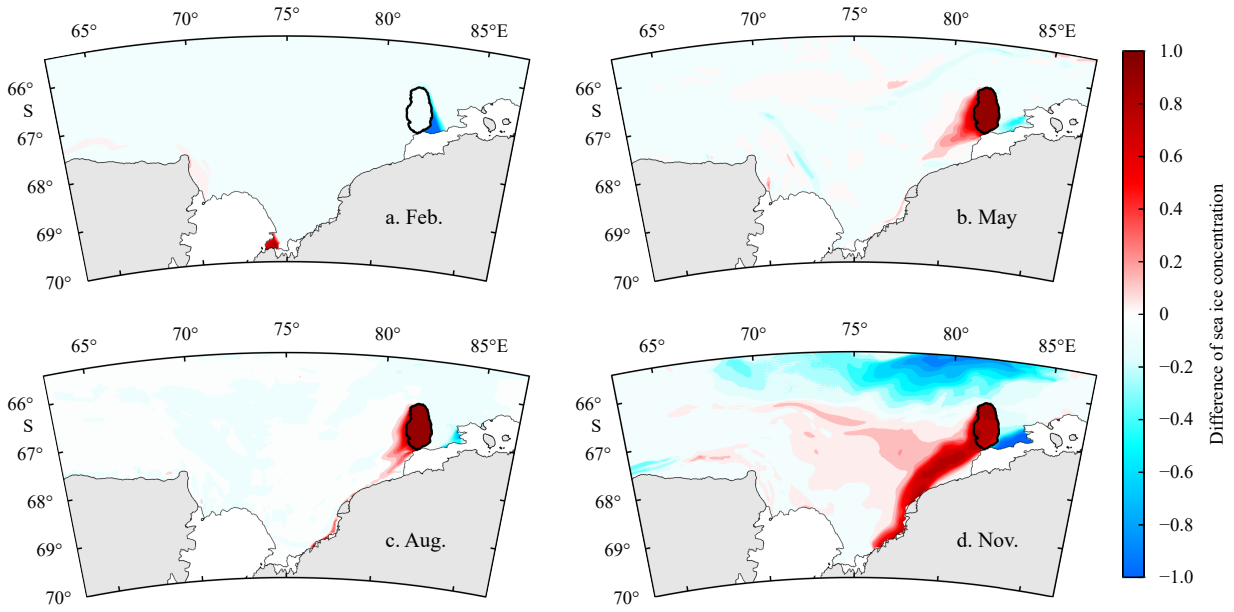


Fig. 11. Difference of sea ice concentration between Exp. 2 and Exp. 1. a. February, b. May, c. August, and d. November. Positive (negative) values represent an increase (decrease) in sea ice after removing Iceberg D15 (closed black curve) from the model.

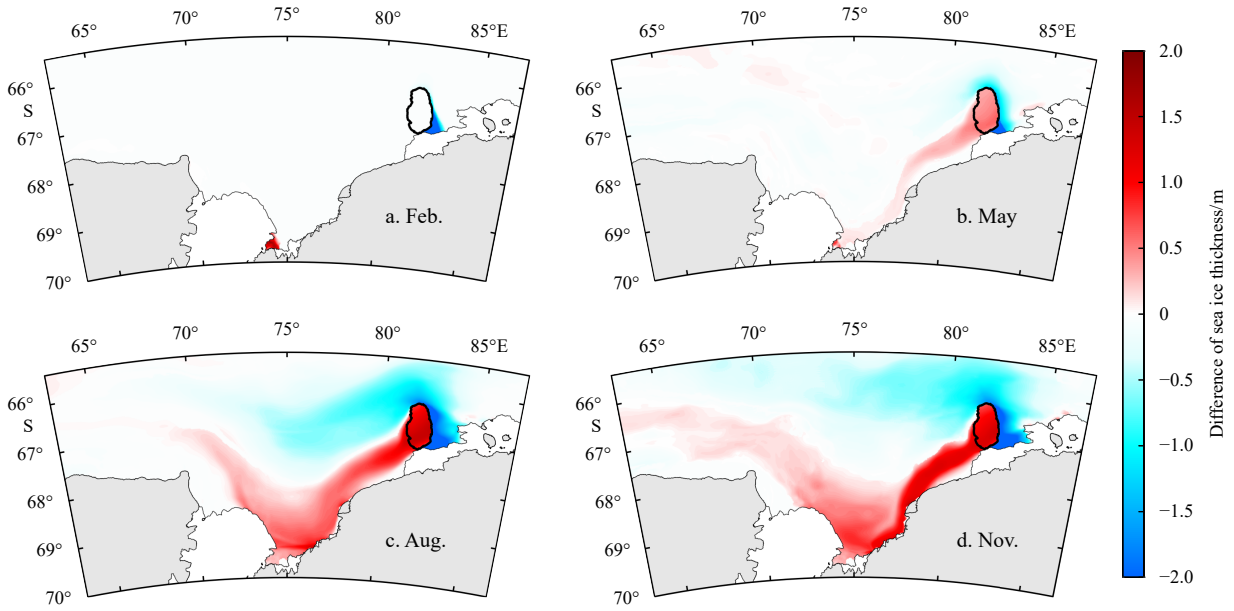


Fig. 12. Difference of sea ice thickness between Exp. 2 and Exp. 1. a. February, b. May, c. August, and d. November. Positive (negative) values represent an increase (decrease) in sea ice after removing Iceberg D15 (closed black curve) from the model. Only areas that passed the significance test at the $p < 0.05$ level are shown.

tions mainly represent pre-1991 conditions before the grounding of Iceberg D15. The Exp. 2 polynya distribution also aligns with earlier numerical modeling results which did not account for Iceberg D15.

The removal of the iceberg considerably changes the areas (Fig. 14a, Table 2) and SIP of the polynyas (Fig. 14b, Table 2). While the MP in the western part of the Prydz Bay experiences only trivial changes (Table 2), the areas and SIP of both BP and DP undergo substantial reductions. In Exp. 2, the total area of BP decreases by approximately 2.83×10^4 km, a 60% reduction compared to Exp. 1, while the area of DP decreases by 2.20×10^4 km^3 (20%). Correspondingly, the total SIP declines by about 4.11×10^{10} m^3 (66%) for BP and 1.52×10^{10} m^3 (52%) for DP. These results emphasize the critical role of Iceberg D15 in polynya and SIP in the region.

4 Conclusions

In this study, we develop a three-dimensional ocean-

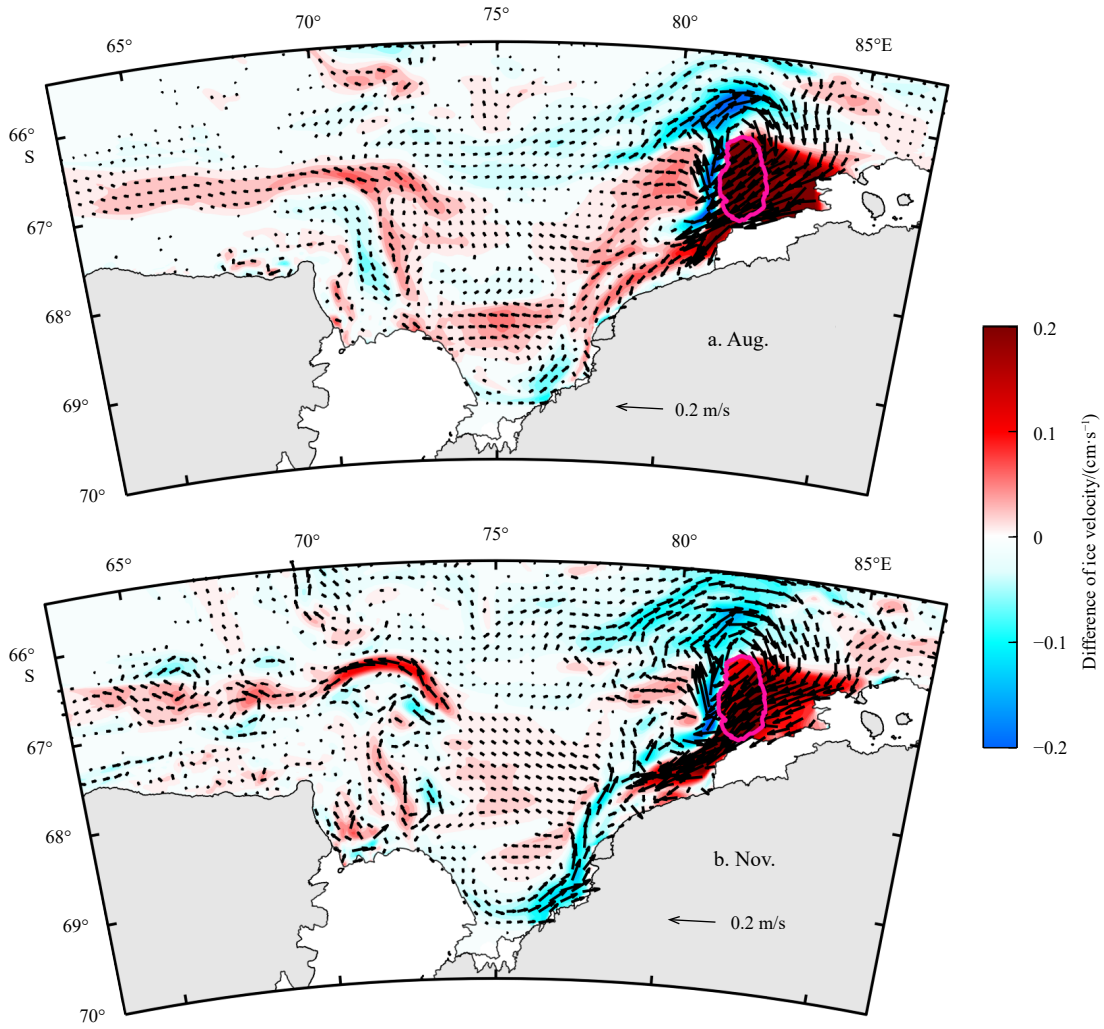


Fig. 13. Difference of ice velocity between Exp. 1 and Exp. 2. a. August, and b. November. Positive (negative) values represent an increase (decrease) in sea ice velocity after removing Iceberg D15 (closed red curve) from the model. Only areas that passed the significance test at the $p < 0.05$ level are shown.

ice shelf-sea ice numerical model in the Prydz Bay and its surrounding seas using ROMS, driven by the climatological forcing from 2013 to 2018. Two numerical experiments are conducted to study the impact of Iceberg D15 on sea ice and polynyas in the model. In Exp. 1, Iceberg D15, grounded on the FLB, is included to demonstrate the performance of the model by comparisons to ADCP velocity data from the 31st Chinese Antarctic Expedition, AMSR-2 remote sensing sea ice concentration and area data averaged over 2013–2018, and evaluations of polynya areas and SIP. Experiment 2, which excludes Iceberg D15, is conducted to assess the impact of the iceberg. By comparing results from the two experiments, the impact of the large grounding Iceberg D15 on sea ice distribution, polynya distributions, and SIP of polynyas in the Prydz Bay is quantitatively examined.

Firstly, Iceberg D15 acts as a critical barrier to sea ice transport, obstructing the sea ice movement outside the WIS into the Prydz Bay. During spring, autumn, and winter, this obstruction leads to sea ice accumulation east of Iceberg D15 and north of the WIS, forming fast ice over 2 m thick. In summer, multi-year sea ice remains at the junction between the southeast of the iceberg and the northwest of the WIS, which disappears when the iceberg is removed.

Secondly, Iceberg D15 considerably impacts sea ice concentration and thickness along the eastern coast of the Prydz Bay in the model. When the iceberg is included, it inhibits ice accumulation in the southeastern bay during spring, resulting in lower sea ice concentrations compared to the central bay and creating ice-free areas that facilitate access for research vessels to the coastal stations such as Zhongshan Station and Davis Station for supplies. Without the iceberg, sea ice moves southwestward along the eastern coastline of the Prydz Bay, leading to small increases in sea ice concentration and widespread growth in ice thickness that extends to the AIS front during autumn and winter. Moreover, the increase in sea ice concentration in spring can extend from the southwest of the iceberg along the coastline to around 75°E.

Thirdly, Iceberg D15 also affects sea ice distribution in a large area to its east and north, changing the sea ice

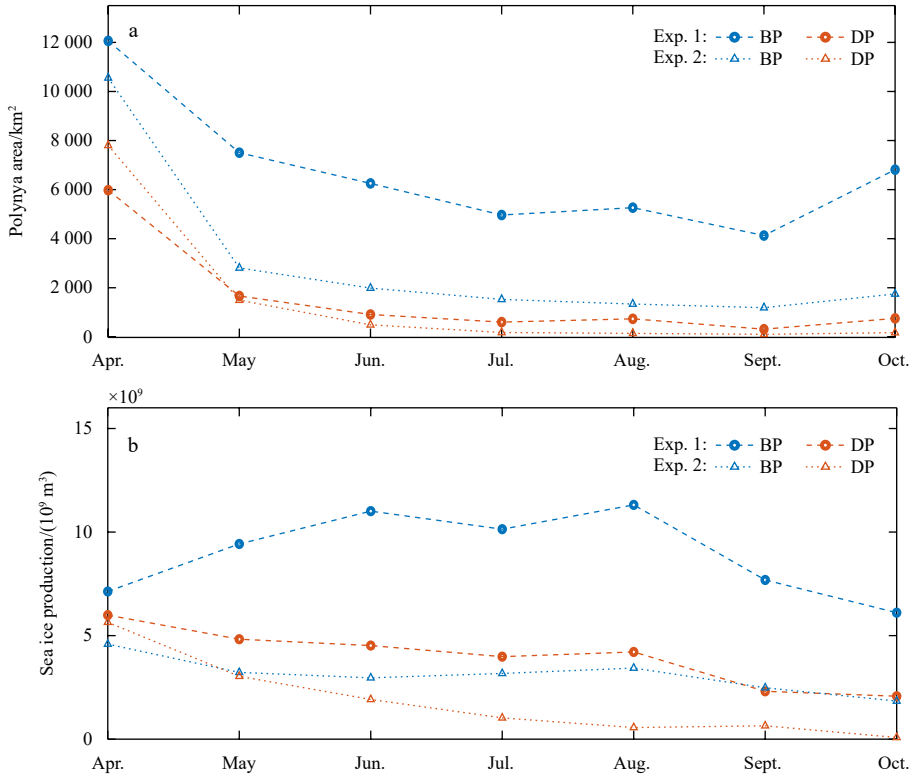


Fig. 14. Areas (a) and SIP (b) of BP and DP for April–October in Exp. 1 and Exp. 2, calculated within the polynya mask shown in Fig. 1.

transport pathways. Its presence allows more sea ice to move westward along the northern edge of the iceberg to the FLB and the north part of the bay. Without the iceberg, sea ice thickness in winter and spring and sea ice concentration in spring decreases over a larger spatial scale, with the reduction extending westward to approximately 70°E.

Finally, Iceberg D15 plays an essential role in modifying the shape and size of BP and DP. Without the iceberg, BP retreats to the southwest of the WIS, and the polynya off the northwest edge of WIS near 83°E expands, resembling the shape observed in remote sensing data before the grounding. The removal of the iceberg increases sea ice thickness in winter and both thickness and concentration in spring across BP and DP regions, leading to smaller polynya extends. Specifically, the total polynya area is reduced by 2.83×10^4 km^2 (60%) and 2.20×10^3 km^2 (20%) from April to October, respectively. Total SIP declines by 4.11×10^{10} m^3 (66%) and 1.52×10^{10} m^3 (52%).

These findings highlight the necessity of adding grounding giant icebergs in the numerical models to accurately represent the distribution of sea ice and polynyas and the SIP of polynyas in the Prydz Bay.

Acknowledgements

We thank the members of Chinese Antarctic Research Expedition and the crew of the R/V *Xuelong* for their professional support in ADCP observations. We thank Saisai Hou for providing the AMSR-2 Antarctic Thin Ice Thickness and Sea Ice Production Data (https://coas.ouc.edu.cn/pogoc/2024/1009/c31871a485693/page.htm). We are grateful to the Chinese National Arctic and Antarctic Data Center (www.chinare.org.cn) for providing the ADCP data, the ECMWF for offering the ERA5 atmospheric reanalysis data (cds.climate.copernicus.eu), the Integrated Climate Data Centre, University of Hamburg, for providing the AMSR-2 sea ice concentration dataset, and the Japan Agency for Marine-Earth Science and Technology for providing the OFES ver. 2 data (www.jamstec.go.jp).

References

Aoki S, Sasai Y, Sasaki H, et al. 2010. The cyclonic circulation in the Australian–Antarctic Basin simulated by an eddy-resolving general circulation model. Ocean Dynamics, 60(3): 743–757, doi: 10.1007/s10236-009-0261-y

Budgell W P. 2005. Numerical simulation of ice-ocean variability in the Barents Sea region: Towards dynamical downscaling. Ocean Dynamics, 55(3): 370–387, doi: 10.1007/s10236-005-0008-3

Dinniman M S, Klinck J M, Smith W O Jr. 2007. Influence of sea ice cover and icebergs on circulation and water mass formation in a numerical circulation model of the Ross Sea, Antarctica. Journal of Geophysical Research: Oceans, 112(C11): C11013, doi: 10.1029/2006JC004036

Galton-Fenzi B K, Hunter J R, Coleman R, et al. 2012. Modeling the basal melting and marine ice accretion of the Amery Ice Shelf. Journal of Geophysical Research:

Oceans, 117(C9): C09031, doi: 10.1029/2012JC008214

Gao Libao, Wei Zexun, Guo Guijun, et al. 2016. Chinese investigation and research in Southern Ocean physical oceanography and meteorology during the Chinese Polar Programs 2011–2015. Advances in Polar Science, 27(4): 209–218, doi: 10.13679/j.advps.2016.4.00209

Han Yuxin, Shi Jiuxin, Hou Saisai, et al. 2022. Numerical simulation of the dynamic effects of grounding icebergs on summer circulation in Prydz Bay, Antarctica. Advances in Polar Science, 33(2): 135–144

Hou Saisai. 2022. Polynyas and Continental Shelf Processes in Eastern Prydz Bay, Antarctica (in Chinese) [dissertation]. Qingdao: Ocean University of China

Hou Saisai, Shi Jiuxin. 2021. Variability and formation mechanism of polynyas in eastern Prydz Bay, Antarctica. Remote Sensing, 13(24): 5089, doi: 10.3390/rs13245089

Hunke E C. 2001. Viscous-plastic sea ice dynamics with the EVP model: Linearization issues. Journal of Computational Physics, 170(1): 18–38, doi: 10.1006/jcph.2001.6710

Hunke E C, Dukowicz J K. 1997. An elastic-viscous-plastic model for sea ice dynamics. Journal of Physical Oceanography, 27(9): 1849–1867, doi: 10.1175/1520-0485(1997)027<1849:AEVPMF>2.0.CO;2

Large W G, Yeager S G. 2009. The global climatology of an interannually varying air-sea flux data set. Climate Dynamics, 33(2): 341–364, doi: 10.1007/s00382-008-0441-3

Li Tian, Liu Yan, Cheng Xiao, et al. 2017. The effect of seafloor topography in the Southern Ocean on tabular iceberg drifting and grounding. Science China: Earth Sciences, 60(4): 4697–4706, doi: 10.1007/s11430-016-9014-5

Li Qun, Wu Huiding, Zhang Lu. 2011. Fine-scale simulation of the seasonal variations of sea ice cover in the Prydz Bay, Antarctic. Haiyang Xuebao (in Chinese), 33(5): 32–38

Lin Yichen, Nakayama Y, Liang Kaixin, et al. 2024. A dataset of the daily edge of each polynya in the Antarctic. Scientific Data, 11: 1006, doi: 10.1038/s41597-024-03848-2

Lin Yichen, Yang Qinghua, Shi Qian, et al. 2023. A volume-conserved approach to estimating sea-ice production in Antarctic Polynyas. Geophysical Research Letters, 50(4): e2022GL101859, doi: 10.1029/2022GL101859

Liu Chengyan, Wang Zhaomin, Cheng Chen, et al. 2017. Modeling modified Circumpolar Deep Water intrusions onto the Prydz Bay continental shelf, East Antarctica. Journal of Geophysical Research: Oceans, 122(7): 5198–5217, doi: 10.1002/2016JC012336

Massom R A, Harris P T, Michael K J, et al. 1998. The distribution and formative processes of latent-heat polynyas in East Antarctica. Annals of Glaciology, 27: 420–426, doi: 10.3189/1998AoG27-1-420-426

Mellor G L, Kantha L. 1989. An ice-ocean coupled model. Journal of Geophysical Research: Oceans, 94(C8): 10937–10954, doi: 10.1029/JC094iC08p10937

Nihashi S, Ohshima K I. 2015. Circumpolar mapping of Antarctic coastal polynyas and Landfast Sea Ice: Relationship and variability. Journal of Climate, 28(9): 3650–3670, doi: 10.1175/JCLI-D-14-00369.1

Nihashi S, Ohshima K I, Tamura T. 2017. Sea-ice production in Antarctic coastal polynyas estimated from AMSR2 data and its validation using AMSR-E and SSM/I-SSMIS data. IEEE Journal of Selected Topics in Applied Earth Observations and Remote Sensing, 10(9): 3912–3922, doi: 10.1109/JSTARS.2017.2731995

Nunes Vaz R A, Lennon G W. 1996. Physical oceanography of the Prydz Bay region of Antarctic waters. Deep-Sea Research Part Ⅰ: Oceanographic Research Papers, 43(5): 603–641, doi: 10.1016/0967-0637(96)00028-3

Ohshima K I, Nihashi S, Iwamoto K. 2016. Global view of sea-ice production in polynyas and its linkage to dense/bottom water formation. Geoscience Letters, 3(1): 13, doi: 10.1186/s40562-016-0045-4

Shchepetkin A F, McWilliams J C. 2005. The regional oceanic modeling system (ROMS): a split-explicit, free-surface, topography-following-coordinate oceanic model. Ocean Modelling, 9(4): 347–404, doi: 10.1016/j.ocemod.2004.08.002

Shi Jiuxin, Dong Zhaoqian, Chen Hongxia. 2013. Progress of Chinese research in physical oceanography of the Southern Ocean. Advances in Polar Science, 24(2): 86–97, doi: 10.3724/sp.j.1085.2013.00086

Shi Jiuxin, Le Kentang, Choi B H. 2002. Circulation and its seasonal variability in region around the Kerguelen Plateau. Acta Oceanologica Sinica, 21(1): 1–17

Shi Jiuxin, Le Kentang, Yu Kangling. 2000. A numerical study of the ice-ocean interaction in the region of Prydz Bay, Antarctica Ⅱ: circulation. Studia Marina Sinica, (42): 22–37

Smith N R, Dong Zhaoqian, Kerry K R, et al. 1984. Water masses and circulation in the region of Prydz Bay, Antarctica. Deep-Sea Research Part A. Oceanographic Research Papers, 31(9): 1121–1147, doi: 10.1016/0198-0149(84)90016-5

Tamura T, Ohshima K I, Fraser A D, et al. 2016. Sea ice production variability in Antarctic coastal polynyas. Journal of Geophysical Research: Oceans, 121(5): 2967–2979, doi: 10.1002/2015JC011537

Tamura T, Ohshima K I, Nihashi S. 2008. Mapping of sea ice production for Antarctic coastal polynyas. Geophysical Research Letters, 35(7): L07606, doi: 10.1029/2007GL032903

Van Achter G, Fichefet T, Goosse H, et al. 2022. Modelling landfast sea ice and its influence on ocean-ice interactions in the area of the Totten Glacier, East Antarctica. Ocean Modelling, 169: 101920, doi: 10.1016/j.ocemod.2021.101920

Wang Chuning, Zhang Zhaoru, Zhong Yisen, et al. 2024. A model study of buoyancy driven cross-isobath transport over the Ross Sea continental shelf break. Journal of Geophysical Research: Oceans, 129(1): e2023JC020078, doi: 10.1029/2023JC020078

Wesche C, Dierking W. 2015. Near-coastal circum-Antarctic iceberg size distributions determined from synthetic aperture radar images. Remote Sensing of Environment, 156:

561–569, doi: 10.1016/j.rse.2014.10.025

Williams G D, Herraiz-Borreguero L, Roquet F, et al. 2016. The suppression of Antarctic bottom water formation by melting ice shelves in Prydz Bay. Nature Communications, 7: 12577, doi: 10.1038/ncomms12577

Zheng Shaojun, Shi Jiuxin. 2011. The characteristic of sea ice growth and melt in the Prydz Bay region, Antarctica. Periodical of Ocean University of China, 41(7): 9–16